# CHAPTER 4: CHEMICAL SYNTHESIS, PHYSICAL CHARACTERIZATION, LINEAR AND NON-LINEAR ABSORPTION MEASUREMENTS OF GRAPHENE OXIDE

## 4.1 Introduction

Graphene oxide (GO) was first produced by chemical oxidation of graphite. Large scale assembly is necessary for the widespread application of the material. Several approaches have been developed to provide a steady supply of GO in large areas and quantities, amenable for mass applications. The current interest in GO has pushed some of the early approaches to large yields, controlled growth and large areas and made it possible to go from micrometre-sized GO sheets to near-mass production of layer-controlled samples.

## 4.2 Preparation and Synthesis Methods of Graphene Oxide

**Chemical oxidation of graphite.** The first, well-known method employed for the synthesis of graphene oxide came in 1859 when British chemist, B. C. Brodie was exploring the structure of graphite by investigating the reactivity of graphite flake [1]. Chemical oxidation of graphite is an established method using concentrated acids (sulphuric acid, nitric acid, and phosphoric acid) and highly oxidizing agents (potassium permanganate and potassium perchlorate). Potassium chlorate; $KClO_3$ was added to a slurry of graphite in fuming nitric acid ($HNO_3$) [1]. Nitric acid is a common oxidizing agent and is known to react strongly with aromatic carbon surfaces, including carbon nanotubes [2, 3]. The reaction results in the formation of various oxide-containing species including carboxyls, lactones, and ketones. Oxidations by $HNO_3$ result in the liberation of gaseous $NO_2$ and/or $N_2O_4$, as demonstrated in Brodie's observation of yellow vapours [4]. Likewise, potassium chlorate is a strong oxidizing agent commonly used in blasting caps or other explosive materials. $KClO_3$ typically is an in situ source of dioxygen, which acts as the reactive species [4]. These were among the strongest

oxidation conditions known at the time, and continue to be some of the strongest used on a preparative scale.

The resulting material composed of carbon, hydrogen, and oxygen, resulting in an increase in the overall mass of the graphite flake. Successive oxidative treatments resulted in a further increase in the oxygen content, reaching a limit after four reactions. The material was dispersible in pure or basic water, but not in acidic media.

**Staudenmaier's method.** Staudenmaier improved Brodie's $KClO_3$-fuming $HNO_3$ preparation by adding the chlorate in multiple aliquots over the course of the reaction with the addition of concentrated sulphuric acid to increase the acidity of the mixture rather than in a single addition [5]. The slight change in the procedure resulted in an overall extent of oxidation; performed more practically in a single reaction vessel [5].

**Hummers' method.** Hummers and Offeman developed an alternate oxidation method by reacting graphite with a mixture of potassium permanganate ($KMnO_4$) and concentrated sulphuric acid ($H_2SO_4$), achieving similar levels of oxidation [6]. The Hummers' method uses a combination of potassium permanganate and sulphuric acid. Though permanganate is a commonly used oxidant, the active species is, in fact, diamanganese heptoxide, as shown in the following chemical reaction scheme:

$$KMnO_4 + H_2SO_4 \rightarrow K^+ MnO_3 + H_3O^+ + 3HSO_4^-$$

$$MnO_3^+ + MnO_4^- \rightarrow Mn_2O_7$$

Diamanganese heptoxide is formed from the reaction of potassium permanganate with sulphuric acid. The bimetallic heptoxide is far more reactive than its monometallic tetraoxide counterpart, and is known to detonate when heated to temperatures greater than 55 $^oC$ or when placed in contact with organic compounds [7, 8].

The original version of the preparation of GO is described as follows: GO was prepared by stirring powdered graphite flake and sodium nitrate into 2.3 litres of sulphuric acid. The ingredients were mixed in a jar that had been cooled to 0 $^{o}$C in an ice-bath as a safety measure. While maintaining vigorous agitation, potassium permanganate was added to the suspension. The rate of addition was controlled carefully to prevent the temperature of the suspension from exceeding 20 $^{o}$C . The ice-bath was then removed and the temperature of the suspension brought to 35 $\pm$ 3$^{o}$C, where it was maintained for 30 minutes. As the reaction progressed, the mixture gradually thickened with a diminishing in effervescence. At the end of 20 minutes, the mixture became pasty with evolution of only a small amount of gas. The paste was brownish grey in colour. At the end of 30 minutes, 4.6 litres of water was slowly stirred into the paste, causing violent effervescence and an increase in temperature to 98 $^{o}$C. The diluted suspension, now brown in colour, was maintained at this temperature for 15 minutes. The suspension was then further diluted to approximately 14 litres with warm water and treated with 3% hydrogen peroxide to reduce the residual permanganate and manganese dioxide to colourless soluble manganese sulphate. Upon treatment with the peroxide, the suspension turned bright yellow. The suspension was filtered, resulting in a yellow-brown filter cake. The filtering was conducted while the suspension was still warm to avoid precipitation of the slightly soluble salt of mellitic acid formed as a side reaction. After washing the yellowish-brown filter cake three times with a total of 14 litres of warm water, the graphitic oxide residue was dispersed in 32 litres of water to approximately 0.5% solids. The remaining salt impurities were removed by treating with resinous anion and cation exchangers. The dry form of graphitic oxide was obtained by centrifugation followed by dehydration at 40 $^{o}$C over phosphorus pentoxide *in vacuo*.

Though others have developed slightly modified versions, the three methods above comprise the primary routes for forming GO. Importantly, it has since been demonstrated that the products of these reactions show strong variance, depending not only on the particular oxidants used, but also on the graphite source and reaction conditions.

Table 4.1 shows a summary of the three main GO synthesis methods described above and some comparisons.

**Table 4.1:** Summary of the conventional synthesis methods of GO.

| Synthesis method | Procedures | Highlights |
|---|---|---|
| Brodie's method | Potassium chlorate; $KClO_3$ was added to a slurry of graphite in fuming nitric acid ($HNO_3$), a common oxidizing agent that reacts strongly with aromatic carbon surfaces. Various oxide-containing species are formed. The resulting product consists of carbon, hydrogen and oxygen, dispersible in pure water. | Very strong oxidation conditions. |
| Staudenmaier's method | Chlorate in multiple aliquots and concentrated sulphuric acid are added in the preparation of KClO3-fuming HNO3 in Brodie's method. | Increase in acidity and hence an overall extent of oxidation in a single reaction. |
| Hummers' method | Graphite was reacted with a mixture of $KMnO_4$ and concentrated $H_2NO_4$. | Diamanganese heptoxide, a very reactive and detonating oxidizing species is formed from the reaction of $KMnO_4$ and $H_2SO_4$. |

## 4.3 Modified Hummers' Method

The text below describes some common methods of synthesizing GO using simplified/improved/modified Hummers' method.

**Modified solution-phase processing.** Natural flake-like graphite was used as the starting material. The oxidation of graphite was carried out by Hummers' method. The delamination of graphite oxide in water was performed by a gentle shaking treatment instead of the conventional ultrasonication to exfoliate the GO sheets [9].

**Oxidation of graphite via bath sonication.** The chemical oxidation of graphite flakes using concentrated $H_2SO_4$, $P_2O_5$, and $K_2S_2O_8$ is replaced with a bath sonication process [10]. The sonication period strongly affects the size of the monolayer GO obtained. The graphite flakes are mixed with concentrated $H_2SO_4$ (12 ml) and kept at 80 $^oC$ for 4.5 hours. The solution is cooled to room temperature and then put into the water-bathed sonication for 1 to 6 hours in concentrated $H_2SO_4$, where the process helps to break the graphite into smaller and thinner flakes. The solution is then diluted with 0.5 l of deionized (DI) water and left overnight. The preoxidized graphite powders were obtained after filtration with porous filters (200 nm pore size). The product is dried in a dry box with gentle baking (70 $^oC$). To exfoliate the graphite flakes into GO sheet, the preoxidized graphite powders are put into concentrated $H_2SO_4$ (120 ml), added $KMnO_4$ (15 mg), following by stirring at room temperature for 2 hours. The solution is diluted with DI water (250 ml) and stirred for 2 hours, and then an additional 0.7 l of DI water is added. Shortly, 20 ml of $H_2O_2$ (30%) is added into the mixture. After setting overnight, upper portions of the solution are collected (unreacted graphite powders precipitated in the bottom of solution) and then centrifuged (at 10,000 rpm). The obtained powders are then dissolved in a 1:10 HCl solution and then centrifuged to remove unwanted metal ions. The powders are then dissolved in DI water and then

centrifuged to remove the acid. The yield of GO sheets for the whole process is about 4.3 wt %.

**Microwave assisted heating method.** Microwave-assisted heating is able to expand the graphite into a thinner layer structure [11]. In this method, a small amount of expandable graphite is sealed in a glass vial, purged with ultrahigh purity nitrogen for 2 hours, and then heated in a microwave oven for less than 2 s. The high polarizabilty of graphene layers causes them to heat rapidly under microwave irradiation. The intercalated species gasify rapidly, and thus fewer point defects are generated by oxidation from intercalated compounds and robustly absorbed oxygen compared to conventional thermal expansion [12-14]. The graphite expands to ~200 times its original volume and is separated into flakes whose thickness is 100 times less than that of the starting material but whose lateral dimension is effectively unchanged. Using such a pre-expanded few layer graphite as a starting material, GO is prepared using Hummers method. Because of the pre-expansion process, high viscosity saturated solutions are produced using only 0.5% (w/w) of microwave expanded graphite, in contrast to conventional methods [13, 15] where ~50 times more graphite is required [13, 15]. The product after oxidation is centrifuged and washed with DI water extensively until the pH stabilizes at ~5.5. No ultrasonication is used [14]. During the water wash, a significant viscosity change is observed, indicating that exfoliation continues in this process. The addition of salt to the resulting solution induces aggregation of the membranes, suggesting that they are charge- stabilized. Only < 1% of unexfoliated graphite is observed.

**"Improved" synthesis.** In this method, the oxidation procedures, where $KMnO_4$ and a 9:1 mixture of concentrated $H_2SO_4/H_3PO_4$ are used to prepared GO [16]. The GO prepared in this way has fewer defects in the basal plane as compared to GO prepared by the conventional Hummers' method. This improved method provides a greater

amount of hydrophilic oxidized graphite material. The GO has a more regular structure with a greater amount of basal plane framework retained and shows an equivalent level of conductivity. This improved method has a simple protocol, higher yield, no toxic gas evolution during preparation, and equivalent conductivity upon reduction and is suitable for preparation material on a large scale.

**Purification by $HNO_3$.** Graphite oxide is synthesized by Hummers' method as usual, except for replacing the purification process with pre-determined concentration of nitric acid, $HNO_3$ [17]. The modification enhances the oxidation of graphite and removes trace impurities of other metal ions.

**Modified chemical exfoliation method.** Three modifications are made in this method:

(1) using graphite with a large lateral size as the starting material to prepare large-area graphite oxide

(2) applying mild oxidation and sonication to avoid the overcracking of graphite during oxidation and exfoliation

(3) using a two-step centrifugation to successively remove thick multilayer flakes and small flakes [18]. Using this method, the largest sheet can reach 40000 $\mu m^2$ in area. Moreover, the area of GO sheets is strongly correlated to the CO content of graphite oxide, and that this can be controlled, to a certain extent, by simply changing the oxidation conditions.

## 4.4 Proposed Method for Graphene Oxide Synthesis

In order to achieve commercial value, the synthesis process of GO needs to be simplistic and cost effective. Chemical synthesis of graphite stands out to be the most popular method employed. It is also an established method using concentrated acids and highly oxidizing agents. The only setback is that, this method requires several steps and temperature controls for the preparation of GO.

Most of the GO reported previously possessed small area and lateral dimensions (side to side), which is approximately 100 $\mu m^2$ and a few nanometres to a few micrometers respectively, [19-23]. It is difficult to produce large area GO due to the unavoidable tearing of GO sheets during the extreme oxidation condition and exfoliation process using ultrasonication. Large area GO has been reported [24] with area < 2000 $\mu m^2$ and lateral dimension of 20 $\mu$m x 40 $\mu$m. Zhou *et. al*. [9] and Su *et. al*. [10] reported the synthesis of ultra-large GO sheets by modifying the oxidation and exfoliation of Hummer's method. Zhao *et. al*. [18] also reported an efficient method to produce large area GO with an area of 7000 $\mu m^2$ and a lateral dimension of up to 100 $\mu$m. However the yield of GO obtained was about 10%, which is very low. Luo *et. al*. [11] reported the formation of GO with high yield, reaching almost 100%. But the size of the GO produced was merely 2000 $\mu m^2$. Furthermore the method involved a long and tedious oxidation process.

Marcono *et. al*. [16] reported the synthesis of GO using an improved Hummer's method. This method introduced a relatively simple oxidation process, with temperature controlled at 50 $^oC$, which was rather low compared with previously reported temperature of 95 $^oC$. However the washing process was time consuming and tedious. Moreover the emphasis of the method was not on producing large area GO but rather more on controlling the level of oxidation and degree of ordering in GO. The conversion rate of graphite to GO was not 100%.

Current popular methods of producing GO using chemical oxidation like Hummers' method [25], Staudeumaier's method [5] and Brodie's method [1] involved tedious and long experimental time. Here, the experimental time does not refer to the time required to oxidize the graphite flakes but rather the time spent by a researcher working on the experiment during the oxidation process. In this work, the long hours of mixing the reactants and cooling or heating the reactants have been reduced from 3–5 hours to less than 5 minutes. Graphite oxidation was achieved simply by adding graphite and potassium permanganate ($KMnO_4$) into concentrated acids (containing
sulfuric acid, with or without phosphoric acid) under constant stirring. The whole process was carried out without any temperature control, neither increasing nor decreasing the temperature. The mixture was stirred at room temperature for up to 3 days to achieve a high degree of oxidation.

Oxidation of graphite was carried out by mixing $H_2SO_4$:$H_3PO_4$ (320:80 mL), graphite flakes, and $KMnO_4$ (18 g) using a magnetic stirrer. After adding all the materials slowly, the one-pot mixture was left for stirring for 3 days to allow the oxidation of graphite. The colour of the mixture changed from dark purplish green to dark brown. Later, $H_2O_2$ solution was added to stop the oxidation process, and the color of the mixture changed to bright yellow, indicating a high oxidation level of graphite. The graphite oxide formed was washed three times with 1 M of HCl aqueous solution and repeatedly with deionized water until a pH of 4–5 was achieved. The washing process was carried out using simple decantation of supernatant via a centrifugation technique with a centrifugation force of 10,000 *g*. During the washing process with deionized water, the graphite oxide experienced exfoliation, which resulted in the thickening of the graphene solution, forming a GO gel.

Figure 4.1 shows the process of synthesizing GO using the proposed improved Hummers' method.

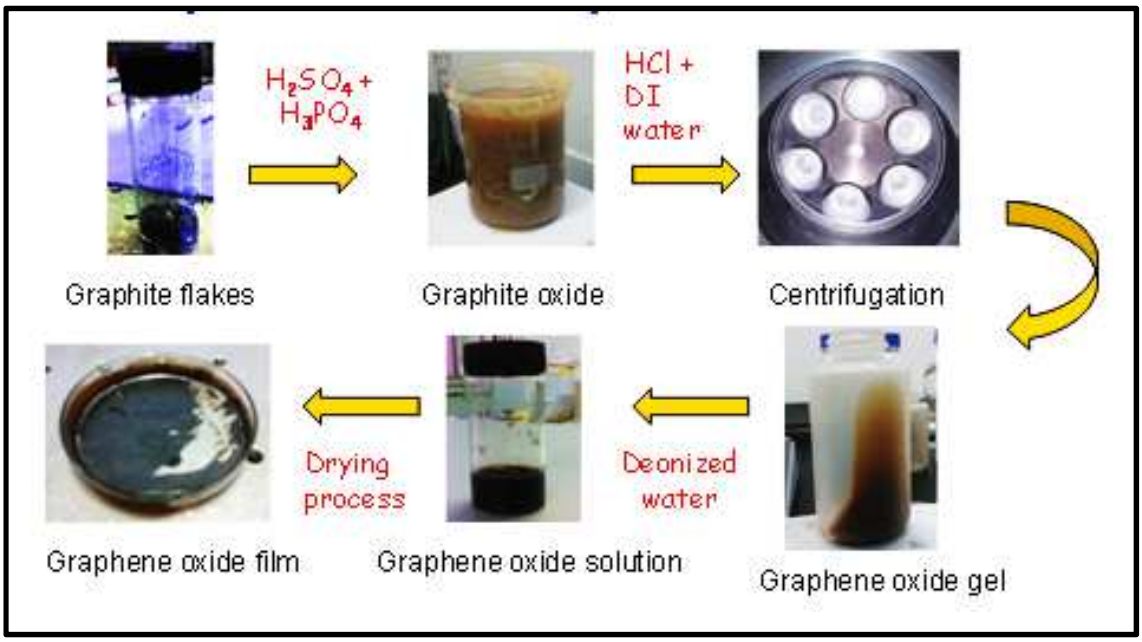


**Figure 4.1:** Process of the proposed GO synthesis method.

## 4.5 Morphological Characterization:

The GO was characterized using a *Thermo Scientific Evolution 300 spectrophotometer* and *Renishaw inVia Raman Microscope* for Raman spectroscopy of dropcast GO on glass substrate at 514nm excitation. Atomic force microscopy (AFM) was performed using *Agilent 5500 (Agilent Technologies, Inc, Santa Clara, CA),* and a tapping mode was employed to determine the thickness of GO. GO was spin-coated at 1500 rpm for 1 minute on a freshly cleaved mica substrate. All the measurements were carried out at room temperature.

A typical tapping mode AFM image and the corresponding height cross-section profile of the GO sheets spin-coated on a mica substrate are shown in Figure 4.2. The GO size ranges from 0.1 to 1.0 $\mu$m. Based on the AFM height profile analysis, the thickness of single layer GO is approximately 1.2 nm. This result is consistent with the thickness of the characteristic single layer GO reported [18] [26]. The height scale in Figure 4.2 (b) has its nominal zero position at a finite height that is approximately 5 nm. It should be

taken as indicating a maximum local thickness of approximately 7 nm, except where a significant wrinkling and folding is occurring.

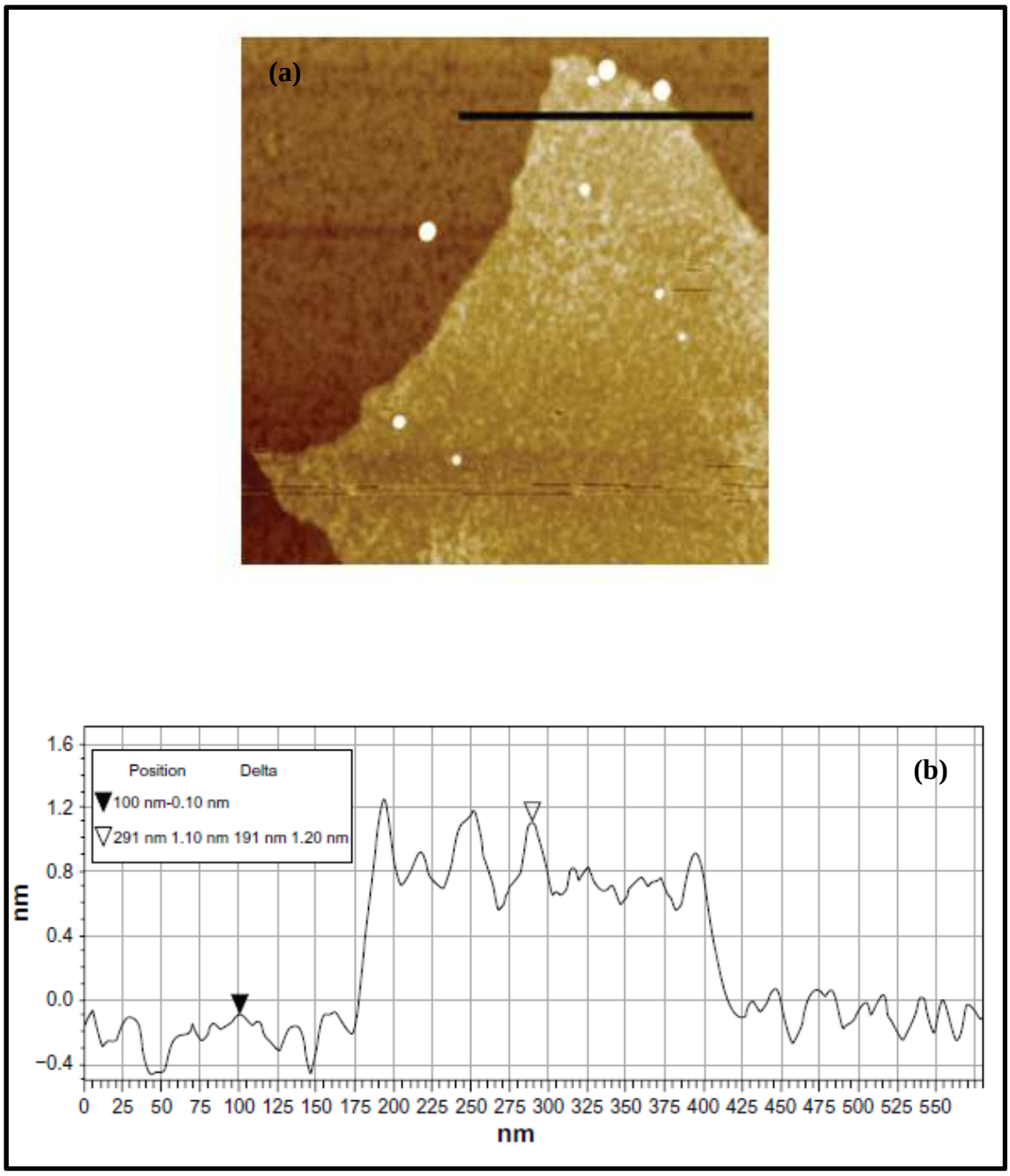


**Figure 4.2:** (a) Tapping mode atomic force microscopy image of single-layer graphene oxide; (b) corresponding height cross-sectional profile with an average thickness of 1.2 nm.

Figure 4.3 shows the Raman spectrum of GO. The spectrum exhibits three main characteristics peaks: the *D* peak arising from the doubly resonant disorder-induced mode (~1353 $cm^{-1}$) due to the stretching of *C*-*C* bond; the *G* peak, a doubly degenerate phonon mode due to the first order scattering of the $E_{2g}$ phonon of $sp^2$ *C* atoms [27] at

the Brillouin zone centre (~1605 $cm^{-1}$); and the 2*D* overtone peak (~2715 $cm^{-1}$) [28-31]. The GO sample shows a prominent *D* peak, indicative of significant structural disorder due to the *O*-incorporation. It is related to the size of the in-plane $sp^2$ domains [32].The increase of the *D* peak intensity indicates forming more $sp^2$ domains. Additionally, the *D* band, is Raman-active at the graphitic edge [28-30] [33]. For small graphene sheets with limited sizes, the *D* band is expected to develop dramatically. The relative intensity ratio of both peaks ($I_D/I_G$) is a measure of disorder degree and is inversely proportional to the average size of the $sp^2$ clusters [32] [34]. Our results show a value of 0.88 for $I_D/I_G$, similar to that of [35]. The 2*D* band at ~2715 $cm^{-1}$, which originates from a two phonon double resonance Raman process and is indicative of crystalline graphitic materials, are highly sensitive to the number of graphene layers, and has been utilised to distinguish the single-layer from few-layer graphene [28-31]. In this work, it is not possible to determine the number of layer in the GO, since the GO solution was drop dried on a silica substrate to prepare a thin film. Hence the Raman spectra is the resultant signal of several stacked GO sheets, each one consisting of a few layers. The steep decrease in intensity and broadening of the 2*D* peak for GO are mainly attributed to the steric effects of oxygen moieties on the stacked layers as well as to the partial amorphization and reduction in $sp^2$ domains. [28, 36].

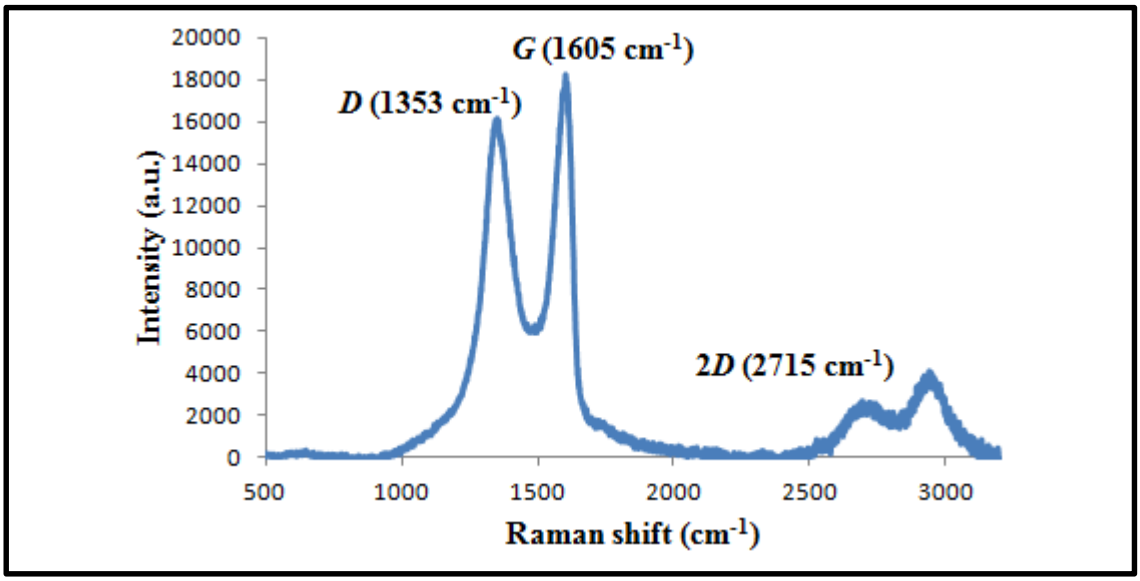


**Figure 4.3:** Raman spectrum of GO coated on a silica substrate.

Figure 4.4 shows the FESEM image of the GO. Some previous work reported that the size of GO reduces with higher degree of oxidation [37, 38]. By using the proposed simplified Hummer's method here, GO with a large lateral dimension is produced with a higher degree of oxidation. This could be attributed to the graphite raw material used for previous works is much smaller size as compared to the graphite flakes used in this work. Also, the graphite may have over-oxidized under high temperature (95°C) as shown in some other works. As for the work here, the optimum oxidation time is 3 days with the GO produced having the largest dimension. A possible mechanism for the formation of large-area GO is the complete oxidation of graphite but not overly oxidized, as it could lead to tearing of the GO sheet. The complete oxidation condition resulted in graphite oxide to be exfoliated easily in large pieces. Another factor that may lead to the formation of large GO is that the reactions were carried out at room temperature. It has been reported that high temperature during the oxidation process reduces the size of the GO produced [37].

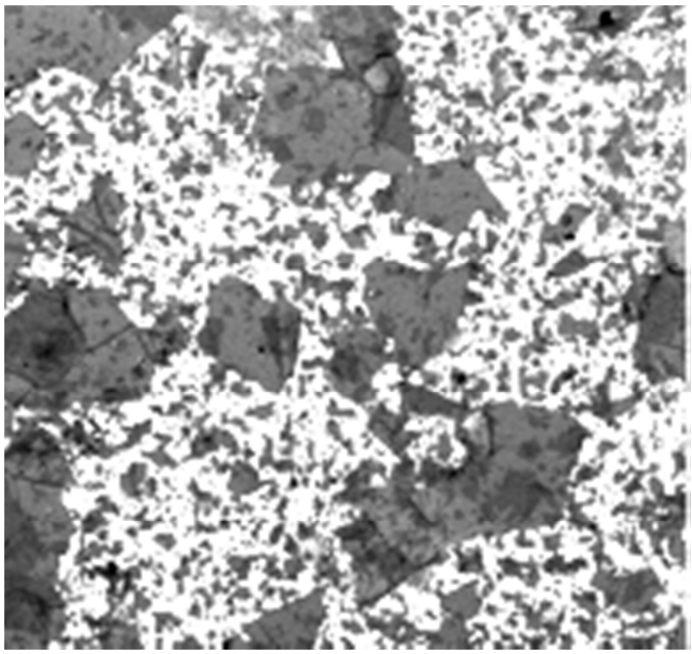

**Figure 4.4:** FESEM image of graphene oxide after 3 days of oxidation.

The XRD pattern of the GO is shown in Figure 4.5. The spectrum shows a distinct diffraction peak at 8.9°, corresponds to a layer to layer of distance (*d*-spacing) of about 1 nm, using Bragg's Law of X-ray Diffraction. This value is very close with the results measured from AFM, indicating the presence of oxygen functionalities at the carbon basal plane via chemical oxidation reaction, which facilitates the hydration and exfoliation of GO sheets.

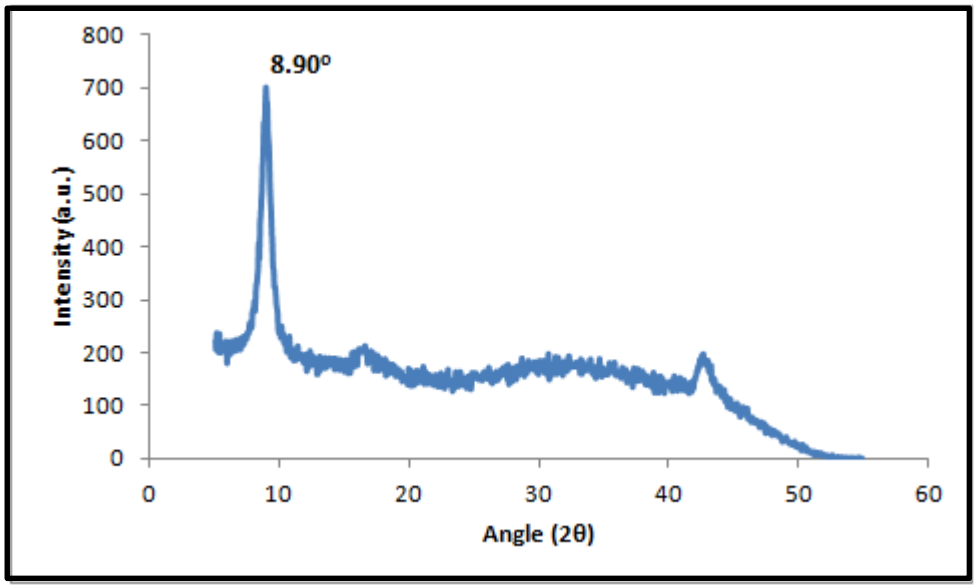


**Figure 4.5:** X-ray diffraction spectrum of graphene oxide.

The characteristic FTIR spectrum of the GO is depicted in Figure 4.6. It is seen with oxygen-containing groups in which the main absorption band at 3360 $cm^{-1}$ is assigned to the O-H group stretching vibrations. This shows that the as-prepared GO here has strong hydrophilicity. The absorption peaks at 1740 $cm^{-1}$, 1640 $cm^{-1}$ and 790 $cm^{-1}$ are due to the C = O stretching of carboxylic or carbonyl moiety functional groups at the edges of the GO sheet. The two absorption peaks at about 1200 $cm^{-1}$ and 1040 $cm^{-1}$ are assigned to the C– O stretching vibrations of epoxy and alkoxy groups respectively. The 1420 $cm^{-1}$ peak is also the stretching vibration of C – O of carboxylic acid.

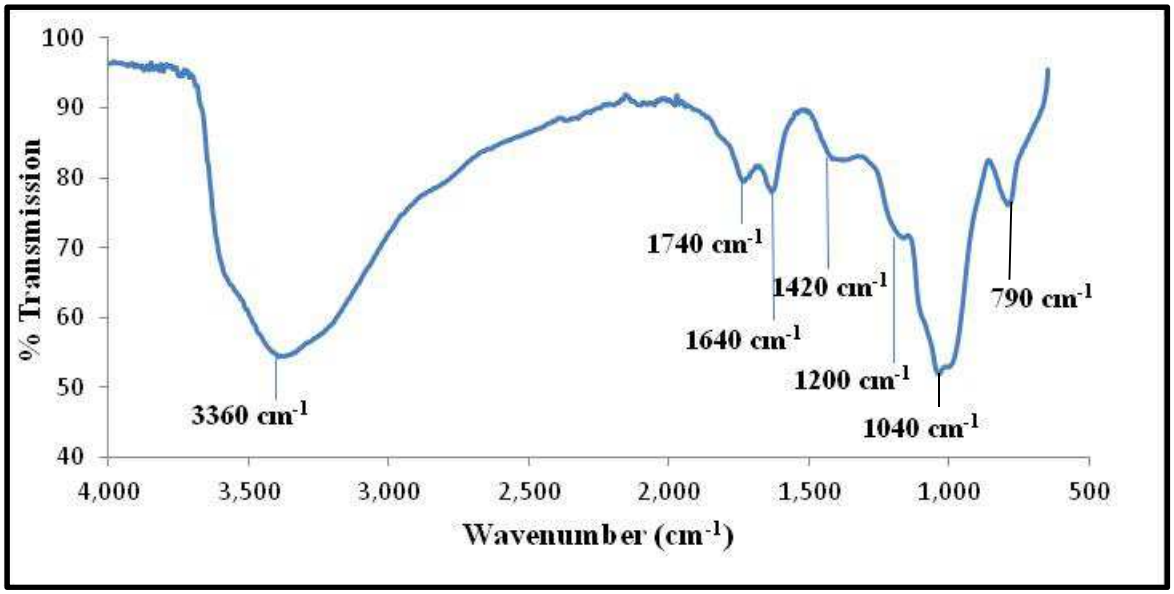


**Figure 4.6:** FTIR spectrum of GO. The presence of oxygen-containing functional groups shows the complete oxidation of graphite.

Figure 4.7 shows the TGA analysis for GO. The first ~ 10% mass loss occurs at room temperature up to ~ 100 °C, which could be atrributed to the evaporation of water molecules [23, 39]. It then significantly decreases from 100 °C to 200 °C (~ 30.44%). The GO slowly further decomposes up to 900 °C. The major mass reduction at ~ 200 °C was caused by pyrolysis of the oxygen-containing functional groups, generating CO, $CO_2$ and $H_2O$ vapours [40].

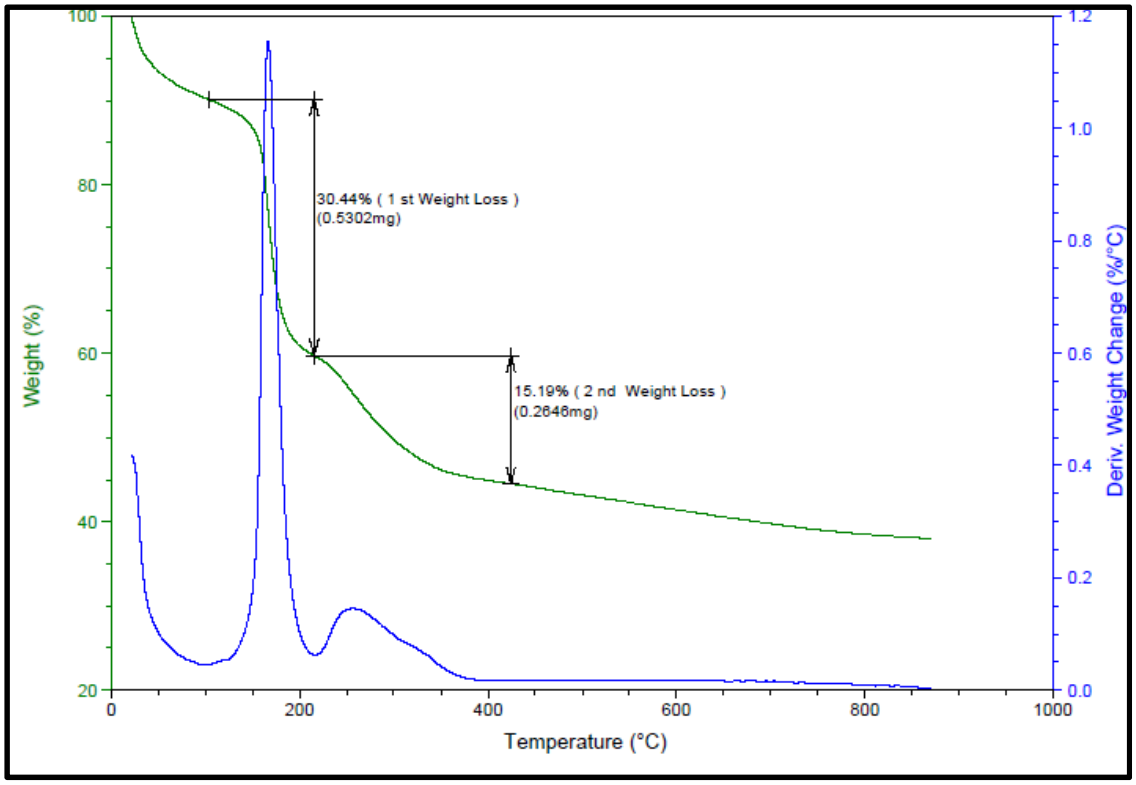


**Figure 4.7:** TGA plot for GO. The GO has a high thermal stability up to 200$^{o}$C.

## 4.6 Nonlinear Absorption Measurements of Graphene Oxide Saturable Absorber

SA devices can be characterized easily, in favour that the key parameters such as saturation intensity, non-saturable absorption, modulation depth etc. can be controlled. Graphene based materials are becoming more and more important in generating pulsed sources and therefore it is desirable to know all the key parameters to determine their role in generating pulses and also to provide customized parameters for certain laser design. In the work here, a wide dynamic range experimental setup is constructed to measure the non-linear absorption of the GO absorber. By using a simple two-level absorber model, the key parameters of a SA are readily available from the measured data. A fitting procedure using the absorber model is used.

Before the nonlinear optical characterization is done, the linear absorption measurement of the GO absorber is first done, as discussed in the following Section 4. 6.1

### 4.6.1 Linear Optical Characterization

Linear optical absorption of the GO absorber is investigated by using *Perkin-Elmer 1050 UV-VIS-NIR spectrophotometer*. Figure 4.8 shows the UV-Visible-NIR absorption spectrum of GO in water. The spectra are plotted in the wavelength range from 200 to 1800 nm for water. An absorption band was observed at 228 nm of excitation, with absorbance intensity of briefly 2.29. This result is in close proximity to that of graphite oxide as reported in [41]. The strong absorption band is due to the $\pi \rightarrow \pi^*$ transitions of aromatic $C = C$ bonds. The plot below 200 nm can be ignored, due to fluctuations in baseline measurement, which is the deionized water. A small ‘shoulder’ is observed at ~300 nm, possibly contributed by the $n \rightarrow \pi^*$ transitions of $C = O$ bonds. Based on the AFM height profile analysis in Section 4.4 (Figure 4.2(b)), the thickness of the GO sample is around 1.2 nm. The result is consistent with the thickness of the characteristic single-layer GO reported.

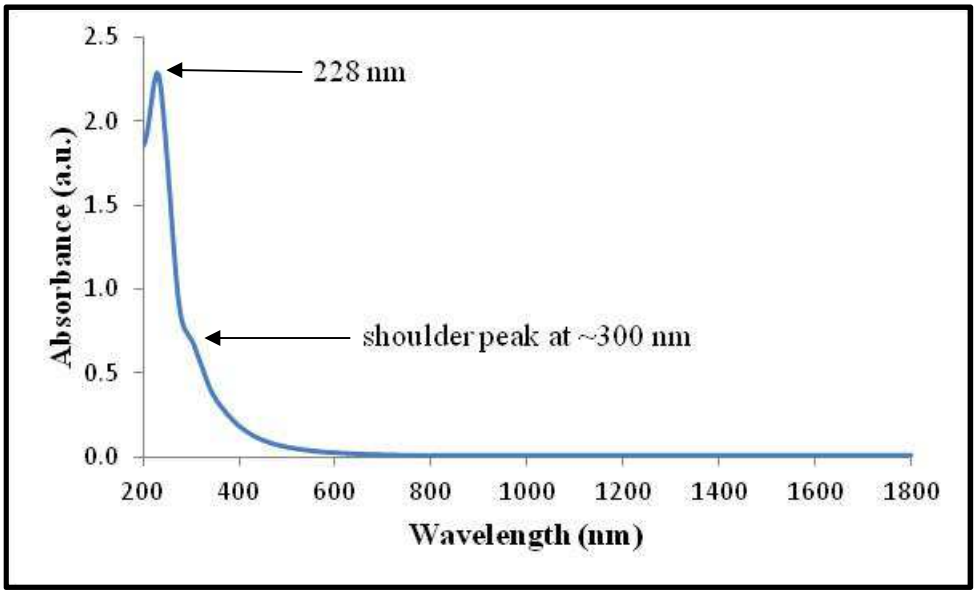


**Figure 4.8:** UV-Visible-NIR absorbance spectra of GO in water.

### 4.6.2 Nonlinear Absorption Measurements

A SA can be characterised by three major parameters:

(i) modulation depth, $\alpha_0$

(ii) saturation fluence, $F_{sat}$

(iii) non-saturable loss, $\alpha_{ns}$

Pump-and-probe measurement is usually used to determine these absorber parameters [6]. The modulation depth $\alpha_0$ is defined as the maximum possible change of optical absorption, $\Delta\alpha$ (or saturable absorption) over the linear absorption of the absorber, $\alpha_{lin}$. It may also be expressed in $\Delta T/T$ or $\Delta R/R$, with $T$ and $R$ being the device transmission and reflectivity respectively, depending on whether the absorber is working in transmission or reflection mode. Non-saturable absorption, $\alpha_{ns}$ is the part of the absorber loss that is present even if the absorber is fully saturated at relatively high intensity. A large $\alpha_{ns}$ will decrease the modulation depth of the device since the linear absorption $\alpha_{lin}$ is the sum of $\Delta\alpha$ and $\alpha_{ns}$. Most often, $\alpha_{ns}$ needs to be minimized for optimised mode-

locking performance. The saturation intensity $I_{sat}$ is defined as the optical intensity (power per unit area) it takes to reduce the absorption of the SA by half its saturable absorption.

A nonlinear absorption experiment, also known as power dependent transmission experiment, is a measurement where the absorption or transmission of a SA device is recorded at different input pump power levels. The pump is normally in the form of short optical pulses to increase the sensitivity of the measurement. The decrease of measured SA absorption at higher intensity reflects the strength of nonlinear absorption of the absorber. In most cases, a two-level model of SA without considering the recovery time can be used to describe the nonlinear behaviour of a SA:

$$\alpha = \frac{\Delta\alpha}{1+I/I_{sat}} + \alpha_{ns} \quad \ldots\ldots (4.1)$$

The equation depicts an ideal fast SA where the absorption responds instantaneously to the incident optical intensity. The meanings of the symbols are the same as described in the above paragraph. Figure 4.9 schematically illustrates the fitting of nonlinear absorption data using the two-level fast absorber model.

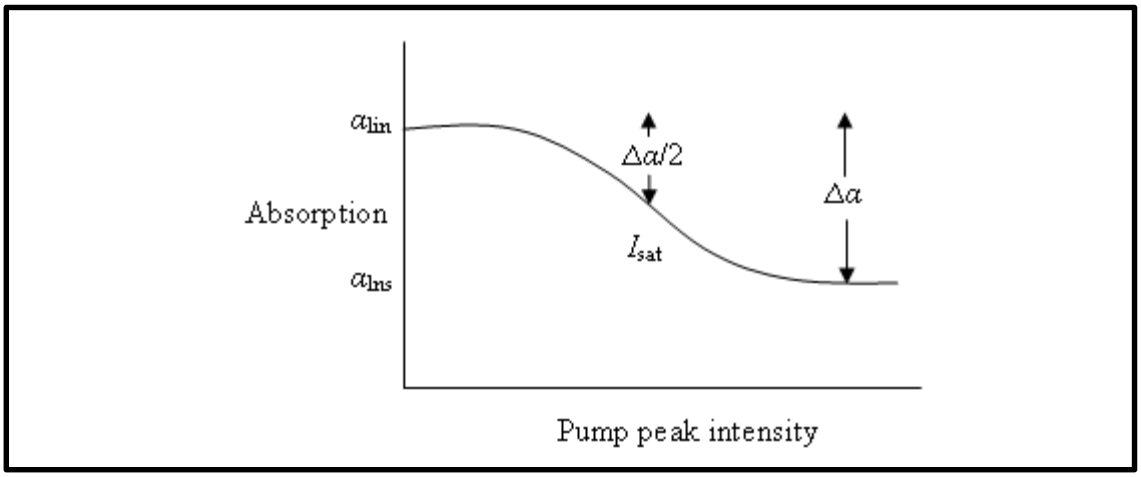


**Figure 4.9:** Fitting of nonlinear absorption using two-level fast absorber model.

The modulation depth in such a case can also be expressed as

$$\alpha_0 = \frac{\Delta\alpha}{\alpha_{lin}} = \frac{\Delta\alpha}{\Delta\alpha + \alpha_{ns}} \quad \ldots\ldots (4.2)$$

Apart from the above mentioned parameters, other properties that are important for a SA absorber device include the wavelength range over which it absorbs light and its damage power threshold.

It is generally expected that the nonlinear absorption of the SA device depends on the duration of the incident pulse. Particularly, when the pulse duration becomes significantly larger than the absorption recovery time, a higher pulse energy is needed to saturate the absorption. It is important that the SA nonlinear response is characterized with the pulse duration and wavelength similar to the conditions when the SA operates in a laser. The correct absorber parameters can then be used in a laser simulation to estimate the steady state output pulse characteristics.

In this work, an experimental setup for measuring the nonlinear response of the GO has been developed. The setup consists of three main sections:

(i) Pulsed laser source

The pulsed laser source used here is a home-made single wall carbon nanotube (SWCNT) mode-locked fibre laser having a pulse duration of ~9 ns, operating at 15.0 MHz, tunable from 1535 nm to 1565 nm. The source has a spectral bandwidth at 1558 nm, achieved by filtering the output of the mode-locked fibre laser using a 3 nm band-pass filter.

(ii) Amplifier

The output pulse from the SWCNT mode-locked laser is amplified in a home-made erbium-doped fibre amplifier (EDFA).

(iii) Measurement unit

The output from the EDFA is divided into two using a 10 dB optical coupler. The 90% power port is used to pump GO assembly while the 10% power port monitors the input power.

The three sections of the setup above are shown in Figure 4.10.

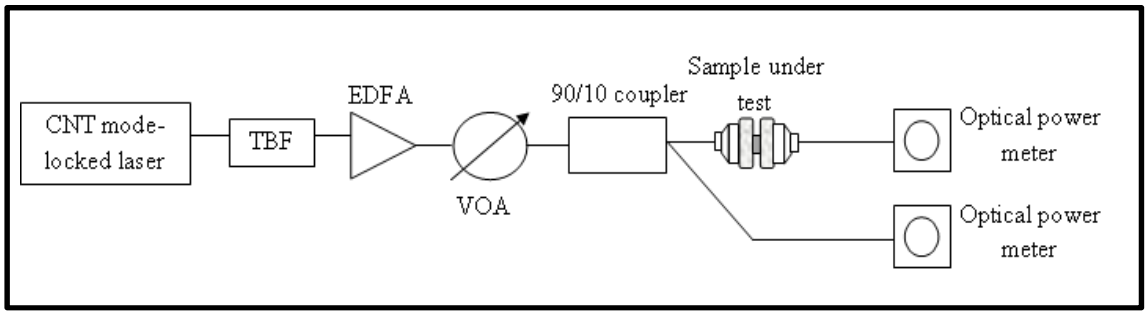


**Figure 4.10:** A schematic illustration for the experimental setup for nonlinear absorption measurements.

The GO, in the form of film, is 'sandwiched' in between two fibre ferrules fixed in a fibre adapter of physical contact (FC/PC).

A schematic of the assembly is shown in Figure 4.11.

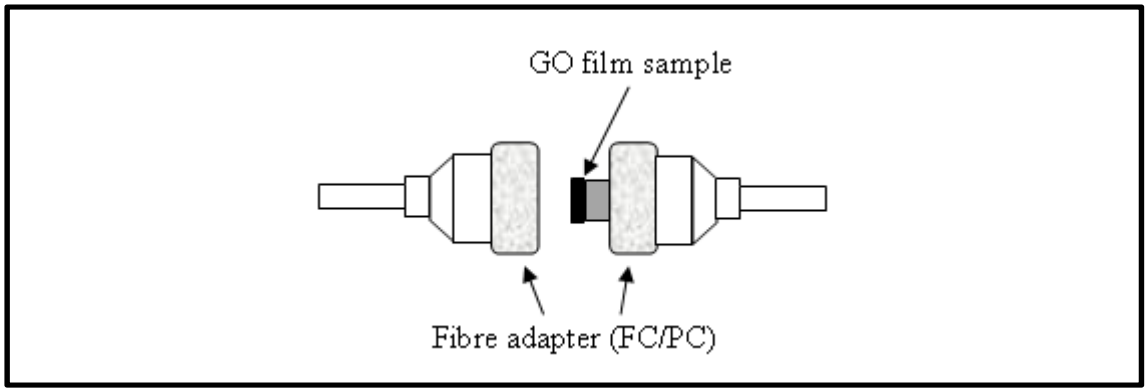


**Figure 4.11:** GO SA device assembly.

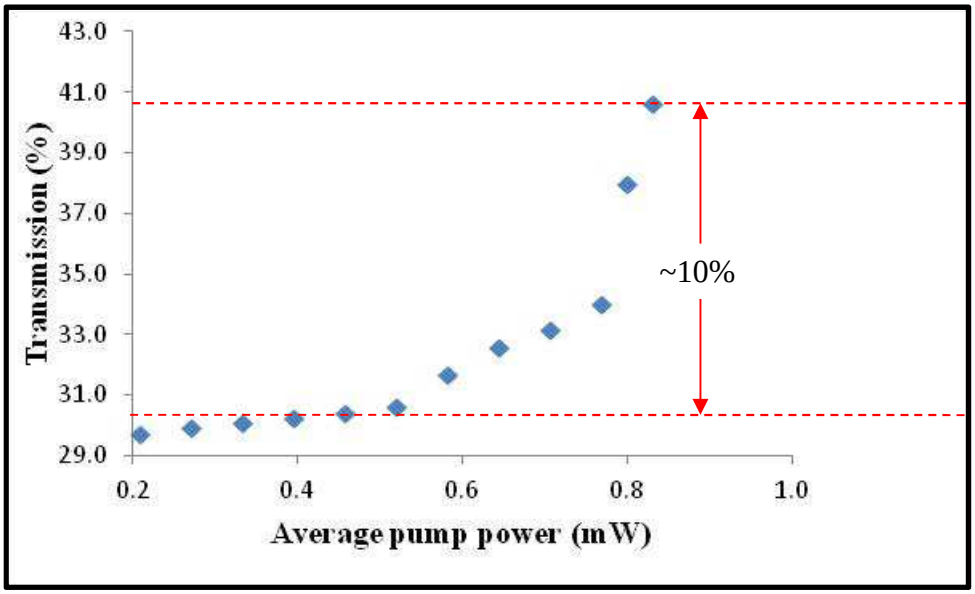


**Figure 4.12:** Transmission of the GO SA device as a function of average pump power.

Figure 4.12 shows the measured transmission as a function of average pump power. At a relatively low input power level, the transmission is nearly independent of pump power. When the incident average power is raised to ~0.8 mW, corresponding to a peak power density of ~6.7 kW/cm$^2$, the transmission increases by ~10% due to absorption saturation. Further increase in transmission is executable; it is only limited by the maximum available pump intensity. The non-saturable insertion loss is about 59.4%. This is tolerable for a relatively large single round-trip gain coefficient [42].

At a pump wavelength of 1558 nm, the total number of pump photons per cm$^2$ per pulse, $n$, at 0.5 mW is

$$n = \frac{0.5\ \text{mW}}{15\ \text{MHz x}\ E_{\text{photon}}\ \text{x}\ A_{\text{eff}}} = 2.96 \text{ x } 10^{14}\ \text{cm}^{-2}$$

The estimated effective mode area, $A_{\text{eff}}$, is 8.825 x 10$^{-7}$ cm$^2$, deduced from the ~10.6 $\mu$m mode diameter of a single mode fibre.

To estimate the non-saturable insertion loss due to the coupling between the fibre adapters, a reference fibre adapters assembly with no GO film in it is used in place of the GO film assembly. The transmission of the empty fibre adapters is ~85%.

The average number of layers participating in the absorption process can be estimated from

$$\tau = \tau_o (1 - \alpha_1)^N \text{ ..... } (4.3)$$

where $\alpha_1$ is the universal absorption of any graphitic materials, which is approximately 2.3% [43]. $\tau_o$ is the transmission of the empty fibre adapters, $\tau$ is the maximum measured transmission and $N$ is the number of layers of the GO.

The total number of photons absorbed by the GO film layers per $cm^2$ per pulse is

$(85 – 40.6)\ \% \times n = 1.34 \times 10^{14}\ cm^{-2}$.

Solving for $N$, it can be estimated that there are ~32 layers of GO that participate in the absorption. The average number of photons absorbed per layer per $cm^2$ per pulse is ~$4.2 \times 10^{10}\ cm^{-2}$.

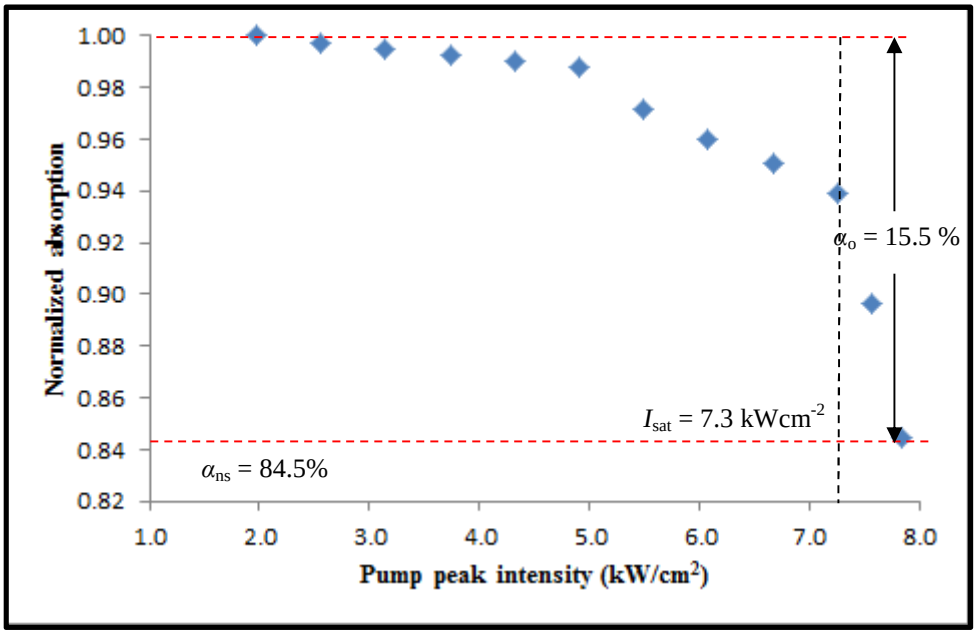


**Figure 4.13:** Normalized absorption as a function of pump peak intensity.

Figure 4.13 shows the fitting curve of the two-level saturable absorber model. The fitting has revealed a saturable absorption of ~15.5% and a saturation intensity of ~7.3 kW/cm$^2$. This corresponds to a ~10% modulation in transmission, as shown in Figure 4.12 previously. Ideally, the absorption at low input intensity should be small with a large modulation depth, i.e. power-dependent change in transmission ($\Delta T$). Repeated measurements at high fluence show no significant degradation of the GO film, indicating good thermal stability of the SA material. The relatively large non-saturable absorption of 84.5% is due to the non-saturated absorbance of the film and the linear divergence loss at the fibre mode coupler, due to the film thickness. The non-saturable loss can be optimized by reducing the thickness of the GO film.

## References


[1] B. C. Brodie, "On the Atomic Weight of Graphite," *Philosophical Transactions of the Royal Society of London,* vol. 149, pp. 249-259, January 1, 1859 1859.

[2] P. V. Lakshminarayanan, H. Toghiani, and C. U. Pittman Jr, "Nitric acid oxidation of vapor grown carbon nanofibers," *Carbon,* vol. 42, pp. 2433-2442, 2004.

[3] N. Zhang, L.-y. Wang, H. Liu, and Q.-K. Cai, "Nitric acid oxidation on carbon dispersion and suspension stability," *Surface and Interface Analysis,* vol. 40, pp. 1190-1194, 2008.

[4] F. A. Cotton, G. Wilkinson, C. A. Murillo, and M. Bochmann, *Advanced Inorganic Chemistry*. Singapore: Wiley India, 2004.

[5] L. Staudenmaier, "Verfahren zur Darstellung der Graphitsäure," *Berichte der deutschen chemischen Gesellschaft,* vol. 31, pp. 1481-1487, 1898.

[6] W. S. Hummers and R. E. Offeman, "Preparation of Graphitic Oxide," *Journal of the American Chemical Society,* vol. 80, pp. 1339-1339, 2013/11/16 1958.

[7] K. R. Koch, "Oxidation by Mn207: An impressive demonstration of the powerful oxidizing property of dimanganeseheptoxide," *Journal of Chemical Education,* vol. 59, p. 973, 2013/11/16 1982.

[8] A. Simon, R. Dronskowski, B. Krebs, and B. Hettich, "The Crystal Structure of Mn2O7," *Angewandte Chemie International Edition in English,* vol. 26, pp. 139-140, 1987.

[9] X. Zhou and Z. Liu, "A scalable, solution-phase processing route to graphene oxide and graphene ultralarge sheets," *Chemical Communications,* vol. 46, pp. 2611-2613.

[10] C.-Y. Su, Y. Xu, W. Zhang, J. Zhao, X. Tang, C.-H. Tsai, and L.-J. Li, "Electrical and spectroscopic characterizations of ultra-large reduced graphene oxide monolayers," *Chemistry of Materials,* vol. 21, pp. 5674-5680, 2009.

[11] Z. Luo, Y. Lu, L. A. Somers, and A. T. C. Johnson, "High Yield Preparation of Macroscopic Graphene Oxide Membranes," *Journal of the American Chemical Society,* vol. 131, pp. 898-899, 2013/11/16 2009.

[12] E. H. L. Falcao, R. G. Blair, J. J. Mack, L. M. Viculis, C.-W. Kwon, M. Bendikov, R. B. Kaner, B. S. Dunn, and F. Wudl, "Microwave exfoliation of a graphite intercalation compound," *Carbon,* vol. 45, pp. 1367-1369, 2007.

[13] O.-Y. Kwon, S.-W. Choi, K.-W. Park, and Y.-B. Kwon, "The preparation of exfoliated graphite by using microwave," *JOURNAL OF INDUSTRIAL AND ENGINEERING CHEMISTRY-SEOUL-,* vol. 9, pp. 743-747, 2003.

[14] X. S. Du, M. Xiao, Y. Z. Meng, and A. S. Hay, "Facile synthesis of exfoliated and highly conductive poly (arylene disulfide)/graphite nanocomposites," *Polymers for Advanced Technologies,* vol. 15, pp. 320-323, 2004.

[15] S. Gilje, S. Han, M. Wang, K. L. Wang, and R. B. Kaner, "A chemical route to graphene for device applications," *Nano letters,* vol. 7, pp. 3394-3398, 2007.

[16] D. C. Marcano, D. V. Kosynkin, J. M. Berlin, A. Sinitskii, Z. Sun, A. Slesarev, L. B. Alemany, W. Lu, and J. M. Tour, "Improved synthesis of graphene oxide," *ACS nano,* vol. 4, pp. 4806-4814.

[17] V. K. Singh, M. K. Patra, M. Manoth, G. S. Gowd, S. R. Vadera, and N. Kumar, "In situ synthesis of graphene oxide and its composites with iron oxide," *New carbon materials,* vol. 24, pp. 147-152, 2009.

[18] J. Zhao, S. Pei, W. Ren, L. Gao, and H.-M. Cheng, "Efficient preparation of large-area graphene oxide sheets for transparent conductive films," *ACS nano,* vol. 4, pp. 5245-5252.

[19] S.-T. Yang, S. Chen, Y. Chang, A. Cao, Y. Liu, and H. Wang, "Removal of methylene blue from aqueous solution by graphene oxide," *Journal of Colloid and Interface Science,* vol. 359, pp. 24-29.

[20] H.-M. Ju, S. H. Huh, S.-H. Choi, and H.-L. Lee, "Structures of thermally and chemically reduced graphene," *Materials Letters,* vol. 64, pp. 357-360.

[21] T. Zhang, D. Zhang, and M. Shen, "A low-cost method for preliminary separation of reduced graphene oxide nanosheets," *Materials Letters,* vol. 63, pp. 2051-2054, 2009.

[22] L. Chen, Z. Xu, J. Li, C. Min, L. Liu, X. Song, G. Chen, and X. Meng, "Reduction and disorder in graphene oxide induced by electron-beam irradiation," *Materials Letters,* vol. 65, pp. 1229-1230.

[23] S. Stankovich, D. A. Dikin, R. D. Piner, K. A. Kohlhaas, A. Kleinhammes, Y. Jia, Y. Wu, S. T. Nguyen, and R. S. Ruoff, "Synthesis of graphene-based nanosheets via chemical reduction of exfoliated graphite oxide," *Carbon,* vol. 45, pp. 1558-1565, 2007.

[24] C. T. Vincent, J. A. Matthew, Y. Yang, and B. K. Richard, "High-throughput solution processing of large-scale graphene," *Nature Nanotechnology,* vol. 4, pp. 25-29, 2008.

[25] W. S. Hummers Jr and R. E. Offeman, "Preparation of graphitic oxide," *Journal of the American Chemical Society,* vol. 80, pp. 1339-1339, 1958.

[26] D. A. Dikin, S. Stankovich, E. J. Zimney, R. D. Piner, G. H. B. Dommett, G. Evmenenko, S. T. Nguyen, and R. S. Ruoff, "Preparation and characterization of graphene oxide paper," *Nature,* vol. 448, pp. 457-460, 2007.

[27] A. C. Ferrari and J. Robertson, "Interpretation of Raman spectra of disordered and amorphous carbon," *Physical review B,* vol. 61, p. 14095, 2000.

[28] A. C. Ferrari, J. C. Meyer, V. Scardaci, C. Casiraghi, M. Lazzeri, F. Mauri, S. Piscanec, D. Jiang, K. S. Novoselov, S. Roth, and A. K. Geim, "Raman Spectrum of Graphene and Graphene Layers," *Physical Review Letters,* vol. 97, p. 187401, 2006.

[29] M. A. Pimenta, G. Dresselhaus, M. S. Dresselhaus, L. G. Cancado, A. Jorio, and R. Saito, "Studying disorder in graphite-based systems by Raman spectroscopy," *Physical Chemistry Chemical Physics,* vol. 9, pp. 1276-1290, 2007.

[30] I. Calizo, A. A. Balandin, W. Bao, F. Miao, and C. N. Lau, "Temperature Dependence of the Raman Spectra of Graphene and Graphene Multilayers," *Nano Letters,* vol. 7, pp. 2645-2649, 2013/10/03 2007.

[31] K. S. Kim, Y. Zhao, H. Jang, S. Y. Lee, J. M. Kim, K. S. Kim, J.-H. Ahn, P. Kim, J.-Y. Choi, and B. H. Hong, "Large-scale pattern growth of graphene films for stretchable transparent electrodes," *Nature,* vol. 457, pp. 706-710, 2009.

[32] Y. Guo, X. Sun, Y. Liu, W. Wang, H. Qiu, and J. Gao, "One pot preparation of reduced graphene oxide (RGO) or Au (Ag) nanoparticle-RGO hybrids using chitosan as a reducing and stabilizing agent and their use in methanol electrooxidation," *Carbon,* vol. 50, pp. 2513-2523.

[33] K. N. Kudin, B. Ozbas, H. C. Schniepp, R. K. Prud'homme, I. A. Aksay, and R. Car, "Raman Spectra of Graphite Oxide and Functionalized Graphene Sheets," *Nano Letters,* vol. 8, pp. 36-41, 2013/10/03 2007.

[34] O. Akhavan and E. Ghaderi, "Escherichia coli bacteria reduce graphene oxide to bactericidal graphene in a self-limiting manner," *Carbon,* vol. 50, pp. 1853-1860.

[35] A. Ganguly, S. Sharma, P. Papakonstantinou, and J. Hamilton, "Probing the thermal deoxygenation of graphene oxide using high-resolution in situ X-ray-based spectroscopies," *The Journal of Physical Chemistry C,* vol. 115, pp. 17009-17019.

[36] M. S. Dresselhaus, A. Jorio, M. Hofmann, G. Dresselhaus, and R. Saito, "Perspectives on Carbon Nanotubes and Graphene Raman Spectroscopy," *Nano Letters,* vol. 10, pp. 751-758, 2013/10/03.

[37] J. Zhao, S. Pei, W. Ren, L. Gao, and H.-M. Cheng, "Efficient Preparation of Large-Area Graphene Oxide Sheets for Transparent Conductive Films," *ACS Nano,* vol. 4, pp. 5245-5252, 2010/09/28 2010.

[38] L. Zhang, J. Liang, Y. Huang, Y. Ma, Y. Wang, and Y. Chen, "Size-controlled synthesis of graphene oxide sheets on a large scale using chemical exfoliation," *Carbon,* vol. 47, pp. 3365-3368, 2009.

[39] S. Park, J. An, J. R. Potts, A. Velamakanni, S. Murali, and R. S. Ruoff, "Hydrazine-reduction of graphite- and graphene oxide," *Carbon,* vol. 49, pp. 3019-3023, 2011.

[40] A. Lerf, H. He, M. Forster, and J. Klinowski, "Structure of Graphite Oxide Revisited," *The Journal of Physical Chemistry B,* vol. 102, pp. 4477-4482, 1998/06/01 1998.

[41] J. I. Paredes, S. Villar-Rodil, A. MartiÌ nez-Alonso, and J. M. D. TascoÌ n, "Graphene Oxide Dispersions in Organic Solvents," *Langmuir,* vol. 24, pp. 10560-10564, 2013/10/03 2008.

[42] K. H. Fong, K. Kikuchi, C. S. Goh, S. Y. Set, R. Grange, M. Haiml, A. Schlatter, and U. Keller, "Solid-state Er:Yb:glass laser mode-locked by using single-wall carbon nanotube thin film," *Optics Letters,* vol. 32, pp. 38-40, 2007/01/01 2007.

[43] A. B. Kuzmenko, E. van Heumen, F. Carbone, and D. van der Marel, "Universal Optical Conductance of Graphite," *Physical Review Letters,* vol. 100, p. 117401, 2008.